Glass-transition properties of Yukawa potentials: From charged point particles to hard spheres

Anoosheh Yazdi,[1,2] Alexei Ivlev,[2] Sergey Khrapak,[2,3] Hubertus Thomas,[2,3] Gregor E. Morfill,[2] Hartmut Löwen,[4] Adam Wysocki,[4,5] and Matthias Sperl[1]

[1]*Institut für Materialphysik im Weltraum, Deutsches Zentrum für Luft- und Raumfahrt, 51170 Köln, Germany*

[2]*Max-Planck-Institut für extraterrestrische Physik, 85741 Garching, Germany*

[3]*Forschungsgruppe Komplexe Plasmen, Deutsches Zentrum für Luft- und Raumfahrt, 82234 Weßling, Germany*

[4]*Institut für Theoretische Physik II: Weiche Materie, Heinrich-Heine-Universität Düsseldorf, Universitätsstrasse 1, 40225 Düsseldorf, Germany*

[5]*Theoretical Soft Matter and Biophysics, Institute for Advanced Simulation and Institute of Complex Systems, Forschungszentrum Jülich, 52425 Jülich, Germany*

(Received 9 August 2013; revised manuscript received 22 May 2014; published 30 June 2014)

The glass transition is investigated in three dimensions for single and double Yukawa potentials for the full range of control parameters. For vanishing screening parameter, the limit of the one-component plasma is obtained; for large screening parameters and high coupling strengths, the glass-transition properties cross over to the hard-sphere system. Between the two limits, the entire transition diagram can be described by analytical functions. Unlike other potentials, the glass-transition and melting lines for Yukawa potentials are found to follow shifted but otherwise identical curves in control-parameter space.

DOI: 10.1103/PhysRevE.89.063105 PACS number(s): 52.27.−h, 64.70.Q−, 64.70.pe, 64.70.ph

I. INTRODUCTION

The physics of ordered (crystals) and disordered (glasses) solid states and their inter-relation has been subject to investigations in various model systems [1,2]. Such model systems capture typical features of more complex matter and often allow for the variation of the interparticle interactions to explore physical regimes otherwise not accessible. A qualitatively strong variation concerns the distinction between hard and soft repulsion as in the Yukawa potential which describes the range from excluded-volume to charge-based interactions.

Yukawa potentials are realized in both colloidal suspensions [3–5] and complex plasmas [2], and since in complex plasmas the damping can be tuned, this offers a way for the comparison of Brownian and Newtonian dynamics with the same particle-particle interaction in experimental systems [6]. While in sterically stabilized colloidal suspensions, the interaction can typically be well approximated by the hard-sphere interaction [1]; for charged particles in suspensions, hard-sphere plus Yukawa interaction is more appropriate. In complex plasmas, the average interparticle distance compared to the particles' diameters is typically large enough to allow for an approximation of pointlike particles, and hence a screened Coulomb potential for point particles is appropriate. In addition to the screening length, in complex plasmas also a second repulsive length scale arises from the nonequilibrium ionization-recombination balance [7,8], which gives rise to a double Yukawa potential at interparticle distances r as

$$\frac{U(r)}{k_{\mathrm{B}}T} = \frac{\Gamma}{r}[\exp(-\kappa r) + \epsilon \exp(-\alpha\kappa r)]\,. \tag{1}$$

Distance r is given in units of the mean interparticle distance $1/\sqrt[3]{\rho}$, with the density $\rho = N/V$ for N particles in a volume V. The coupling parameter is $\Gamma = Q^2\sqrt[3]{\rho}/(k_{\mathrm{B}}T)$, with the charge Q, and $\kappa = 1/(\lambda\sqrt[3]{\rho})$ is the inverse of the screening length λ. The second (longer-ranged) Yukawa potential is specified by a relative strength ϵ, and a relative inverse screening length $\alpha < 1$. In the limit of vanishing screening, one recovers the one-component plasma (OCP), the simplest model that exhibits characteristics of charged systems [9]. Motivated by the success of mode-coupling theory for ideal glass transitions (MCT) for the hard-sphere system (HSS), cf. Ref. [10], in the following, the glass-transition is calculated within MCT [11]. Since for time-reversible evolution operators, i.e., Newtonian and Brownian dynamics, the glassy dynamics within MCT are identical [12], the calculations are applicable to both complex plasma and charged colloids.

II. METHODS

Considering N pointlike particles interacting via the pairwise repulsive potential in Eq. (1), we investigate the glass transitions in two cases: the single Yukawa ($\epsilon = 0$) and the double Yukawa potential ($\epsilon > 0$). Within MCT, the glass transition is defined as a singularity of the form factor $f_q = \lim_{t\to\infty}\phi_q(t)$ that is the long-time limit of the density autocorrelation function. In the liquid state, f_q is zero, while in the glass state, $f_q > 0$. At the transition singularity, the form factors adopt their critical values $f_q^c \geqslant 0$. f_q is the solution of [13]

$$\frac{f_q}{1-f_q} = \mathcal{F}_q[f_k]\,, \tag{2}$$

which is the long time limit of the full MCT equations of motion. f_q is distinguished from other solutions of the Eq. (2) by its maximum property; thus it can be calculated using the iteration $f_q^{(n+1)}/(1-f_q^{(n+1)}) = \mathcal{F}_q[f_k^{(n)}]$ [14] with $f_k^{(0)} = 1$ and the memory kernel given by

$$\mathcal{F}_q[f_k] = \frac{1}{16\pi^3}\int d^3k\,\frac{S_qS_kS_p}{q^4}(\mathbf{q}\cdot\mathbf{k}c_k + \mathbf{q}\cdot\mathbf{p}c_p)^2 f_k f_p, \tag{3}$$

where $\mathbf{p} = \mathbf{q} - \mathbf{k}$; all wave vectors are expressed in normalized units. The only inputs to Eq. (3) are the static structure factors S_q. The number density does not appear explicitly in the kernel $\mathcal{F}_q$, since all length scales are expressed in units of $1/\sqrt[3]{\rho}$. The

Fourier-transformed direct correlation functions c_q are related to structure factors through the Ornstein-Zernike (OZ) relation

$$\gamma_q = \frac{c_q^2}{1 - c_q}, \tag{4}$$

where the spatial Fourier transform of γ_q is $\gamma(r) = h(r) - c(r)$ and $h(r)$ is the total correlation function, which is related to structure factor through $S_q = 1 + h_q$. We close the equations by the hypernetted-chain (HNC) approximation,

$$c(r) = \exp\left[-U(r)/(k_B T) + \gamma(r)\right] - \gamma(r) - 1\,, \tag{5}$$

where $U(r)$ is the interaction potential. It was found earlier that HNC captures well various structural features for repulsive potentials, especially for the OCP [15]. For the HSS, the quality of HNC is known to be inferior to the Percus-Yevick (PY) approximation in certain thermodynamic aspects [9], so we expect HNC to vary in performance for different parameter regions of the Yukawa potentials in Eq. (1).

We solve Eqs. (4) and (5) by iteration and use the usual mixing method in order to ensure convergence [9]. We iterate n times from an initial guess, $c^{(0)}(r)$, until a self-consistent result is achieved, i.e.,

$$\left[\int_0^R |c^{(n+1)}(r) - c^{(n)}(r)|^2\, \mathrm{d}r\right]^{1/2} < \delta, \tag{6}$$

with $\delta = 10^{-5}$, where R is the cutoff length of $c(r)$. We employ $R = 47.1239$ and a mesh of size $M = 2396$ points. Consequently, the resolutions in real and Fourier spaces are $\Delta r = R/M = 0.0197$ and $\Delta q = \pi/R = 0.0667$, respectively. We use an orthogonality-preserving algorithm for the numerical calculation of Fourier transforms [16]. For a particular κ we begin the computation of $c(r)$ at a small coupling parameter Γ, successively increase Γ, and use the outcome as an initial guess for the subsequent calculation.

III. SINGLE YUKAWA POTENTIAL

A. Glass-transition diagram

The MCT results for the single Yukawa case are shown in Fig. 1. The filled circles for different Γ and κ indicate the glass transition points calculated as the boundary between vanishing and finite solutions for f_q from Eq. (2). For $\kappa \to 0$, the glass transition for the OCP limit is found at $\Gamma^c_{\mathrm{OCP}} = 366$. When screening is introduced for $\kappa > 0$, the glass-transition line moves to higher critical coupling strengths $\Gamma^c(\kappa)$. Figure 1 shows for reference the melting curve for weakly screened Yukawa systems, described by $\Gamma(\kappa) = 106\, e^{\kappa}/(1 + \kappa + \kappa^2/2)$ [17,18]. This expression has been suggested originally on the basis of Lindemann-type arguments; cf. Ref. [19]. The Lindemann criterion states that the liquid-crystal phase transition occurs when in the crystal the root-mean-squared displacement $\sqrt{\langle \delta r^2 \rangle}$ of particles from their equilibrium positions reaches a certain fraction of the mean interparticle distance. Within the simplest one-dimensional harmonic approximation this yields the scaling $U''(r = 1)\langle \delta r^2 \rangle / k_B T \simeq$ const., where primes denote the second derivative with respect to distance. Applied to the Yukawa interaction this leads to the melting curve above, where the value of the constant is determined from the condition $\Gamma \simeq 106$ at melting of the OCP system ($\kappa = 0$).[1] This expression for the melting curve is widely used due to its particular simplicity and reasonable accuracy: Deviations from numerical simulation data of Ref. [20] do not exceed several percent, as long as $\kappa \lesssim 8$. Moreover, similar arguments can be used to reasonably describe freezing of other simple systems, e.g., Lennard-Jones-type fluids [21]. Remarkably, when comparing the predicted glass transition with the melting curve, one observes that both transition lines run in parallel. The glass-transition line is described by the function

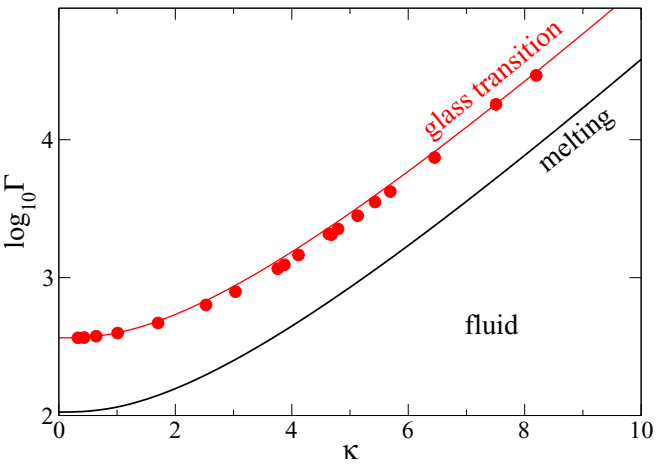

FIG. 1. (Color online) Glass-transition diagram for the single Yukawa potential (filled circles). Transition points are shown together with the full curve exhibiting Eq. (7). For comparison, a similar curve is shown for the melting of the crystal.

$$\Gamma^c(\kappa) = \Gamma^c_{\mathrm{OCP}}\, e^{\kappa}(1 + \kappa + \kappa^2/2)^{-1}, \tag{7}$$

which is shown as solid line in Fig. 1; i.e., the glass transition is found at 3.45 of the coupling strength of the melting curve. An additional rationalization of Eq. (7) using further MCT results is found below in the Appendix.

The fit quality given by Eq. (7) is remarkable for two distinct reasons: First, the potential changes quite drastically along the line from a long-ranged interaction at low κ to the paradigmatic hard-sphere system at very large κ to be detailed below. Such simplicity along control-parameter-dependent glass-transition lines is not to be expected and not observed for other potentials, cf. the square-well system [22,23]. Second, the nontrivial changes along the transition lines are apparently quite similar for the transition into ordered and disordered solids alike, and Eq. (7) applies to both. For the mentioned square-well system, ordered and disordered solids have no such correlation [23].

Since both MCT and the structural input involve approximations, typically the glass transitions are found for higher couplings than predicted; the deviation is around 10% in the densities for the HSS [11]. While one can expect that absolute values for transition points need to be shifted to match experimental values [10], the qualitative evolution of glass-transition lines with control parameters is usually quite

[1]Note that $\Gamma_0 \simeq 172$ if the Wigner-Seitz radius $a = \sqrt[3]{3/4\pi\rho}$ is used as a unit length instead of $1/\sqrt[3]{\rho}$.

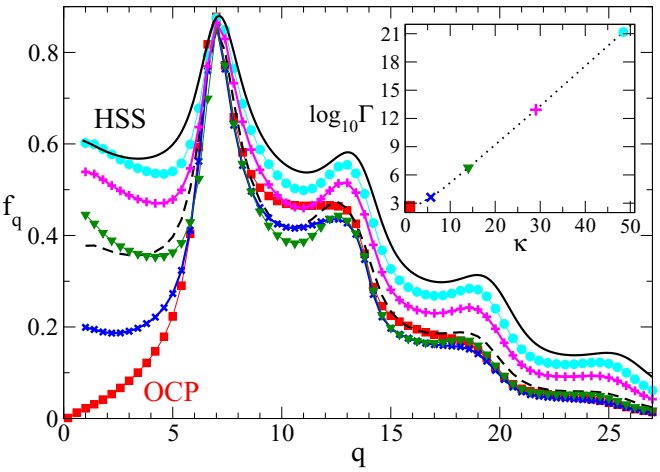

FIG. 2. (Color online) Critical glass-form factors f_q for the glass transition in the single Yukawa system. For increasing screening parameter κ, the inset shows the location of the respective transition points on the MCT-transition line, cf. Fig. 1, with the same symbols as in the main panel. The full curve shows the solution for the HSS within the HNC approximation. The result for HSS within the PY approximation [14] is shown as a dashed line.

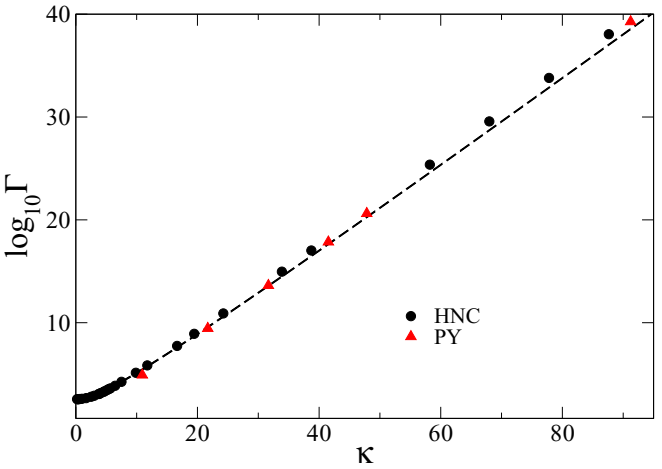

FIG. 3. (Color online) Comparison in the glass-transition line between HNC (bullets) and PY (triangles) for the structure-factor input to the glass-transition calculations. Equation (7) is shown as a dashed curve.

accurate and even counterintuitive phenomena like melting by cooling have been predicted successfully [22]. Hence, we assume the description of the liquid-glass transitions in the single Yukawa system to be qualitatively correct.

B. Glass-form factors

The different points on the glass-transition lines is discussed in detail in the following. For the well-known case of the glass transition in the HSS, the critical form factors are shown by a full curve in Fig. 2. Unlike earlier results calculated for S_q within the PY approximation [14], here we also show the HSS within the HNC approximation to be consistent with the Yukawa results. The control parameter for the HSS is the packing fraction $\varphi = \rho(\pi/6)\,d^3$ with the hard-core diameter d as the unit of length and a nontrivial value for ρ. For HNC, the transition point is found at a packing fraction of $\varphi^c_{\rm HSS} = 0.525$. This value as well as the behavior of f_q in Fig. 2 is very close in HNC and the PY approximation where $\varphi^c_{\rm HSS} = 0.516$ [14].

It is seen in Fig. 2 that the distribution of f_q is dominated by a peak at interparticle distances which indicate the cage effect [11,14]; oscillations for higher wave vectors follow this length scale in a way similar to the static structure factor. For both PY and HNC, the peak positions for f_q coincide; for the principal peak even the peak heights are almost identical. For HNC, the f_q are typically above the PY solutions, resulting in a 10% larger half-width of the distribution of the f_q for the HNC. The predicted deviations between HNC and PY are mostly indistinguishable when comparing to experiments except for the small-q limit where experimental results favor the PY-MCT calculation, cf. [11,24]. Hence, the HNC approximation is suited reasonably well to describe the Yukawa potential over a wide range of κ. The results for the transition line in Fig. 1 agree well with the results from the PY calculation which are shown for selected values of κ in Fig. 3. While both PY and HNC results deviate from Eq. (7) for large κ, there is no apparent disagreement between both approximations regarding the overall evolution of the glass-transition line.

For the Yukawa potential, overall the critical form factors exhibit similar features as for the HSS. Unlike the HSS, in the OCP limit the form factors vanish for the limit $q \to 0$. This anomaly for charged systems corresponds to the small wave-vector behavior in the static structure $S_q \propto q^2$ for $q \to 0$ [9]. Since in the OCP, mass and charge fluctuations are proportional to each other, the conservation of momentum implies the conservation of the microscopic electric current and hence no damping of charge fluctuations in the long wavelength limit. Considering Eq. (3) we demonstrate that $f_q \propto q^2$ for small wave vectors.

Denoting θ as the angle between $\mathbf{q}$ and $\mathbf{k}$ we can expand the direct correlation functions a Taylor expansion as

$$c_{|\mathbf{q}-\mathbf{k}|} = c_k - q\,\cos\theta\, c_k' + \tfrac{1}{2}q^2\cos^2\theta c_k'' - \tfrac{1}{6}q^3\cos^3\theta c_k''', \quad (8)$$

where the primes represent the respective first, second, and third derivatives of c_k with respect to k. Substituting Eq. (8) into Eq. (3) leads to

$$\mathcal{F}_q[f_k] = S_q\alpha + q^2 S_q\beta + \mathcal{O}(q^3), \quad (9a)$$

where [25]

$$\alpha = \frac{1}{4\pi^2}\int_0^\infty dk k^2 S_k^2 \left(c_k^2 + \frac{2}{3}kc_kc_k' + \frac{1}{5}k^2 c_k'^2\right) f_k^2 \quad (9b)$$

and

$$\beta = \frac{1}{4\pi^2}\int_0^\infty dk k^2 S_k^2 \left(\frac{1}{3}c_k'^2 + \frac{1}{28}k^2 c_k''^2 + \frac{2}{5}kc_k'c_k'' + \frac{1}{3}c_kc_k'' + \frac{1}{15}kc_kc_k''' + \frac{1}{21}k^2 c_k'c_k'''\right) f_k^2\,. \quad (9c)$$

The term linear in q in Eq. (9a) vanishes. Similarly, the small-q expansion of the static structure factor in the OCP limit reads [26]

$$S(q) = \frac{q^2}{k_D^2} + \frac{q^4}{k_D^4}[c^R(0) - 1] + \mathcal{O}(q^6), \quad (10)$$

where $k_D^2 = 4\pi\Gamma$ represents the inverse Debye length in the OCP limit, and $c^R(q) = c(q) - c^S(q)$ is the regular term of the direct correlation function, assuming that at large distances particles can only be weakly coupled, which creates the singular term $c^S(q) = -U(q)/k_BT$. From Eqs. (9a) and (10) we get

$$\mathcal{F}_q = q^2\frac{\alpha}{k_D^2} + q^4\left[\frac{\beta}{k_D^2} + \frac{\alpha}{k_D^4}(c^R(0) - 1)\right] + \mathcal{O}(q^6)\,. \quad (11)$$

From Eq. (2) one can conclude that f_q has the same limit as $\mathcal{F}_q$; hence we have shown that $f_q \propto q^2$ for vanishing q.

For nonvanishing screening, $\kappa > 0$, the small-q behavior of the form factors is characterized by finite intercepts at $q = 0$. This regular behavior is ensured by the $q \to 0$ limit of $c_q^S = -4\pi\Gamma/(q^2 + \kappa^2)$. For larger wave vectors, $q \gtrsim 7$, the f_q first decrease in comparison to OCP—cf. $\kappa = 5.7$ (×) and 14.0 (▼) in Fig. 2—before increasing beyond the OCP result for $\kappa \gtrsim 30$. For very large screening, the form factors of the Yukawa potential apparently approach the HSS case.

C. Hard-sphere limit

By setting $U(d_{\rm eff})/k_BT \sim 1$ for $\epsilon = 0$ in Eq. (1) one can define an effective diameter that becomes a well-defined hard-core diameter for $\kappa \to \infty$ for values of Γ along the transition line; cf. Fig. 4. Along the glass-transition line $\Gamma^c(\kappa)$, the effective packing fraction and diameter are given (with logarithmic accuracy) by

$$\varphi_{\rm eff}^c = \frac{\pi}{6}\left(\frac{\ln\Gamma^c}{\kappa}\right)^3, \quad d_{\rm eff}^c = \ln\Gamma^c/\kappa\,, \quad (12)$$

where only the definition of the packing fraction has been used. Figure 5 displays the effective packing fractions along the single Yukawa transition line up to $\kappa \approx 100$. For small κ, the large effective diameter yields considerable overlaps among the particles and hence a packing fraction beyond unity. The effective hard-sphere diameter can be seen in the inset of Fig. 5. For $\kappa \gtrsim 40$ the Yukawa potential's effective diameter $d_{\rm eff}^c$ reaches its asymptotic value. Together with the findings

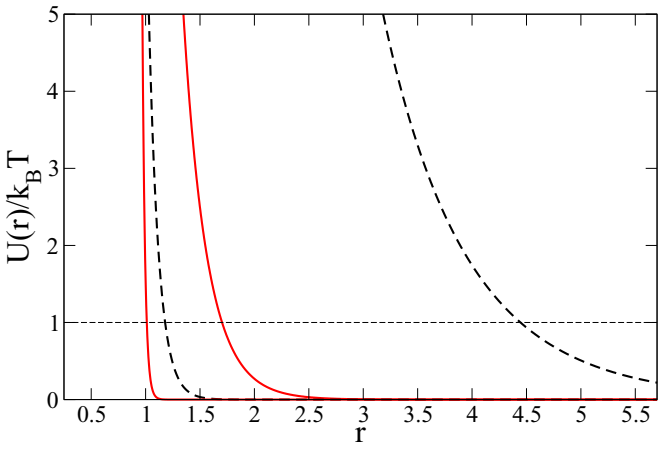

FIG. 4. (Color online) Evolution of the single Yukawa potential along the glass-transition line in Fig. 1. The potentials are shown from right to left for $(\kappa,\Gamma) = (1.01,396)$, $(3.87,1240)$, $(9.87,1.34\times10^5)$, and $(38.71,1.06\times10^{17})$.

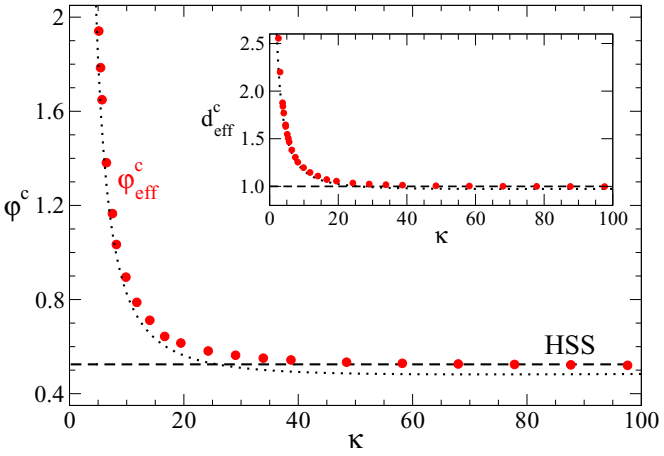

FIG. 5. (Color online) Effective packing fraction $\varphi_{\rm eff}^c$ for Yukawa potentials along the transition line in Fig. 1. The horizontal dashed line shows the HSS-HNC limit of $\varphi_{\rm HSS}^c = 0.525$. The inset shows the effective hard-sphere diameter, $d_{\rm eff}^c = \ln\Gamma^c/\kappa$ equivalent to the effective densities. In both plots, the dotted curves display the small-κ asymptotes derived from Eq. (7).

on the f_q this establishes the crossover of the glass-transition properties of the Yukawa system to the hard-sphere limit. The relation in Eq. (7) fits effective diameters and densities well for smaller $\kappa \lesssim 10$ and underestimates the calculated values for larger κ, as expected.

IV. DOUBLE YUKAWA POTENTIAL

A. Glass-transition diagrams

Progressing towards the double Yukawa potentials, we show in Fig. 6 the results of MCT calculations for the same relative screening $\alpha = 0.125$ and a weak ($\epsilon = 0.01$) as well as a strong ($\epsilon = 0.2$) second repulsion. In both cases, for small κ the transition lines start at OCP and follow the single Yukawa line. After a crossover regime, for $\kappa \gtrsim 15$ for $\epsilon = 0.01$ and $\kappa \gtrsim 10$ for $\epsilon = 0.2$, the transitions are described well by rescaling the original single Yukawa results according to

$$\Gamma' = \Gamma/\epsilon, \quad \kappa' = \kappa/\alpha\,. \quad (13)$$

In Fig. 6, scaling by Eq. (13) is demonstrated by transforming the MCT results for $\epsilon = 0$ (full circles) into a rescaled version (open circles) for $\epsilon = 0.2$ which compares well to the full MCT calculation for the double Yukawa potential (diamonds). Similarly, formula (7) can be used to describe all double Yukawa results for small screening lengths and the results for large screening lengths by scaling Eq. (7) with Eq. (13). The dotted and dashed curves in Fig. 6 exhibit the scaled curves for $\epsilon = 0.01$ and 0.2, respectively. The linear combination of the analytical descriptions for both length scales reads

$$\Gamma^c(\kappa)/\Gamma_{\rm OCP}^c = [e^{-\kappa}(1+\kappa+\kappa^2/2) + \epsilon\, e^{-\kappa\alpha}(1+\kappa\alpha+\kappa^2\alpha^2/2)]^{-1} \quad (14)$$

and is demonstrated by the solid line for $\epsilon = 0.01$ in Fig. 6. It is seen that Eq. (14) describes the MCT results for double Yukawa potentials for the entire range of control parameters κ, Γ, α, and ε, including crossover regions. In conclusion,

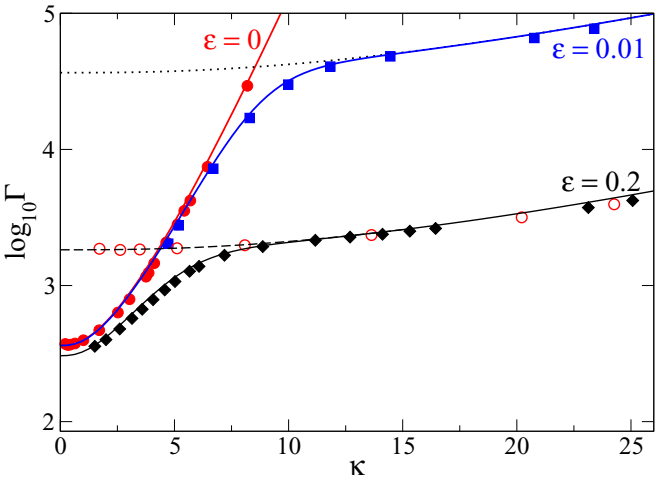

FIG. 6. (Color online) Glass-transition diagram for double Yukawa potentials with $\alpha = 0.125$, $\epsilon = 0.2$ (diamonds) and 0.01 (squares). The single Yukawa data (filled circles) are shown together with the analytical description by Eq. (7) (solid curve labeled $\epsilon = 0$). The single Yukawa points are scaled according to Eq. (13) for $\epsilon = 0.2$ and shown by open circles. Dotted and dashed curves represent scaled versions of Eq. (7) for $\epsilon = 0.01$ and $\epsilon = 0.2$, respectively. The solid curves labeled $\epsilon = 0.01$ and $\epsilon = 0.2$, respectively, show the solution of Eq. (14).

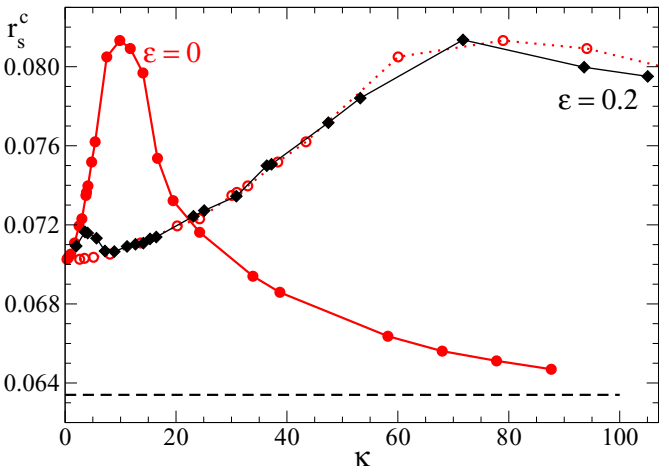

FIG. 7. (Color online) Localization length for single Yukawa (full circles) and double Yukawa (diamonds) potential with $\alpha = 0.125$ and $\epsilon = 0.2$. The open circles show the single Yukawa data scaled according to Eq. (13). The horizontal dashed line shows the HSS limit for r_s^c.

the MCT predictions for both single and double Yukawa potentials can be rationalized by a single analytical formula (7), which traces the melting curve, captures the interplay between large and small repulsive length scales, and extends for all parameters from OCP to HSS.

B. Localization lengths

Another length scale resulting from the dynamical MCT calculations is given by the localization length [11]. It is defined from the long-time limit of the mean-squared displacement $\delta r^2(t) = \langle |r(t) - r(0)|^2 \rangle$ as $r_s^c = \sqrt{\lim_{t\to\infty} \delta r^2(t)/6}$. For the glass transition in the HSS, MCT predicts a localization length within HNC of $r_s^c/d = 0.0634$. This scale is quite close to the classical result of a Lindemann length [19].

For the single and double Yukawa potentials, the evolution of the localization length with κ is demonstrated in Fig. 7. From a value of $r_s^c = 0.070$ for OCP, the localization lengths increase for the single Yukawa potential, reach a maximum around $\kappa \approx 10$, and decrease to the values for HSS for large κ. While the complexity of the combined nonlinear functionals for HNC and MCT do not allow for a rigorous and transparent analytical derivation of the evolution of the localization length, the results can be interpreted as follows: Starting from the OCP glass, increasing the screening (i.e., higher κ) reduces the cage-stabilizing influence of neighbors further away, thus causing the localization to grow above its OCP value. Starting at the HSS glass, reducing the stiffness of the interaction gradually leads to somewhat larger freedom of an otherwise trapped particle in the cage and hence a higher localization length. Both trends together yield a maximum.

The localization lengths for the double Yukawa system follow the single Yukawa results for small $\kappa \lesssim 5$ as observed in Fig. 6 and hence increase; for $\kappa \gtrsim 5$, the double Yukawa system approaches the scaled single Yukawa results shown by the circles. For larger κ, the evolution follows the scaled single Yukawa results and while deviating for $\kappa \gtrsim 50$ from the scaled results, a scaled maximum is reached around $\kappa \approx 80$.

Altogether, the variation of the localization lengths is around 10% which is small compared to other glass-transition diagrams [23]. Hence we conclude that for both single and double Yukawa potentials the MCT results for the localization length are always close to the values usually assumed for the Lindemann criterion.

V. CONCLUSION

In summary, we have demonstrated above the full glass-transition diagram for the single and double Yukawa systems. While some parallel running lines for limited parameter ranges have been shown earlier for logarithmic core potential plus Yukawa tail [27,28], here we describe the transition diagrams by analytical formulas. In particular it could be shown how the HSS limit continuously evolves into the OCP limit. We have shown that the glass-transition lines resulting from the combination of HNC and MCT—two rather complex nonlinear functionals—can be described analytically over their entire range from the OCP limit for small κ to the HSS limit for large κ. Qualitatively, the behavior of the transition line can be estimated by the Lindemann criterion for melting [19], while quantitatively, glass transition and crystal melting follow remarkably similar trends for stronger coupling.

It is important to note that the present calculations were performed for point particles with various degrees of charging and screening. The limit of the HSS emerges from that calculations without actual excluded volume in the potentials. With the important difference of a finite hard-sphere radius being present, the possibility that in addition to a Coulomb crystal a dilute system of charges may also form a Coulomb glass was explored in the restricted primitive

model for a mixture of charged hard spheres [29] and the hard-sphere jellium model [30] as well as for a system of charged hard spheres to describe charge-stabilized colloidal suspensions [31]. In conclusion, the present calculations offer exhaustive analytical descriptions for glass transitions over a wide range of quite different interaction potentials. The predictions should motivate data collapse from computer simulation and different experimental model systems in order to confirm or challenge the unified picture presented above.

ACKNOWLEDGMENTS

Financial support within the ERC (Advanced Grant INTERCOCOS, Project No. 267499) is gratefully acknowledged.

APPENDIX: EFFECTIVE POTENTIAL

Aside from the variations discussed above, it is seen in Figs. 2 and 7 that the overall changes in the localization lengths and short-range changes in the glass-form factors along the transition lines are small. We use that finding in the following to explain why the glass-transition lines follow Eq. (7) closely.

Let us define as in Ref. [9] a potential of mean force,

$$\psi(r) = -k_B T \ln g(r), \tag{A1}$$

from the pair-distribution function $g(r)$ which is the Fourier transform of S_q. Suppose particle 1 and 2 are separated by the distance r and particle 1 remains fixed while particle 2 changes its position by a small value dr, where also all the other particles in the system remain fixed. The change in the pair interaction potential between particles 1 and 2 can be calculated via the expansion

$$\frac{U(r+dr)}{k_B T} - \frac{U(r)}{k_B T} = -\frac{1+\kappa r}{r^2}\Gamma e^{-\kappa r} dr + \frac{2+2\kappa r+\kappa^2 r^2}{2r^3}\Gamma e^{-\kappa r} dr^2 + \ldots. \tag{A2}$$

The change in $\psi(r)$ is equivalent to the sum of the changes in the pairwise interactions between all the particles in the system and particle 2. Due to symmetry the first term on the right-hand side of Eq. (A2) is irrelevant for the sum. In a strongly coupled Yukawa system, the interactions between the particles are dominated by those at mean interparticle distances [21], i.e., $r \approx 1$. The change in the potential of the mean force is then approximately proportional to the second term in Eq. (A2),

$$d\psi \propto \Gamma e^{-\kappa}(1+\kappa+\kappa^2/2). \tag{A3}$$

By inferring from Figs. 2 and 7 that the average cage around typical particles is the same at all transition points, $d\psi$ can be assumed approximately constant. Hence, at the glass-transition points, the average particle in an average cage experiences the same forces along the line of glass transitions described by

$$\Gamma \propto \frac{e^{\kappa}}{1+\kappa+\kappa^2/2}, \tag{A4}$$

which is identical to Eq. (7). While the prefactor remains to be calculated from the microscopic theory, one can understand the functional form of Eq. (7) from a similar argument as the Lindemann criterion used to derive the analytical description of the melting line.

[1] P. N. Pusey and W. van Megen, Nature (London) **320**, 340 (1986).
[2] A. V. Ivlev, H. Löwen, G. E. Morfill, and C. P. Royall, *Complex Plasmas and Colloidal Dispersions* (World Scientific, Singapore, 2012).
[3] F. Bitzer, T. Palberg, H. L. R. Simon, and P. Leiderer, Phys. Rev. E **50**, 2821 (1994).
[4] C. Beck, W. Härtl, and R. Hempelmann, J. Chem. Phys. **111**, 8209 (1999).
[5] M. Heinen, A. J. Banchio, and G. Naegele, J. Chem. Phys. **135**, 154504 (2011).
[6] T. Gleim, W. Kob, and K. Binder, Phys. Rev. Lett. **81**, 4404 (1998).
[7] S. A. Khrapak, A. V. Ivlev, and G. E. Morfill, Phys. Plasmas **17**, 042107 (2010).
[8] A. Wysocki, C. Räth, A. V. Ivlev, K. R. Sütterlin, H. M. Thomas, S. Khrapak, S. Zhdanov, V. E. Fortov, A. M. Lipaev, V. I. Molotkov *et al.*, Phys. Rev. Lett. **105**, 045001 (2010).
[9] J.-P. Hansen and I. R. McDonald, *Theory of Simple Liquids* (Academic, London, 1986), 2nd ed.
[10] M. Sperl, Phys. Rev. E **71**, 060401 (2005).
[11] W. Götze, *Complex Dynamics of Glass-Forming Liquids: A Mode-Coupling Theory* (Oxford University Press, Oxford, 2009).
[12] G. Szamel and H. Löwen, Phys. Rev. A **44**, 8215 (1991).
[13] U. Bengtzelius, W. Götze, and A. Sjölander, J. Phys. C **17**, 5915 (1984).
[14] T. Franosch, M. Fuchs, W. Götze, M. R. Mayr, and A. P. Singh, Phys. Rev. E **55**, 7153 (1997).
[15] K.-C. Ng, J. Chem. Phys. **61**, 2680 (1974).
[16] F. Lado, J. Comput. Phys. **8**, 417 (1971).
[17] O. S. Vaulina and S. A. Khrapak, Zh. Eksp. Teor. Fiz. **117**, 326 (2000) [JETP **90**, 287 (2000)].
[18] O. Vaulina, S. Khrapak, and G. Morfill, Phys. Rev. E **66**, 016404 (2002).
[19] F. A. Lindemann, Phys. Z. **11**, 609 (1910).
[20] S. Hamaguchi, R. T. Farouki, and D. H. E. Dubin, Phys. Rev. E **56**, 4671 (1997).
[21] S. A. Khrapak, M. Chaudhuri, and G. E. Morfill, J. Chem. Phys. **134**, 241101 (2011).
[22] K. Dawson, G. Foffi, M. Fuchs, W. Götze, F. Sciortino, M. Sperl, P. Tartaglia, T. Voigtmann, and E. Zaccarelli, Phys. Rev. E **63**, 011401 (2000).
[23] M. Sperl, Phys. Rev. E **69**, 011401 (2004).
[24] W. van Megen, Transp. Theory Stat. Phys. **24**, 1017 (1995).
[25] M. Bayer, J. Brader, F. Ebert, E. Lange, M. Fuchs, G. Maret, R. Schilling, M. Sperl, and J. P. Wittmer, Phys. Rev. E **76**, 011508 (2007).

[26] M. Baus and J. P. Hansen, Phys. Rep. **59**, 1 (1980).
[27] G. Foffi, F. Sciortino, P. Tartaglia, E. Zaccarelli, F. LoVerso, L. Reatto, K. A. Dawson, and C. N. Likos, Phys. Rev. Lett. **90**, 238301 (2003).
[28] F. Sciortino, S. Mossa, E. Zaccarelli, and P. Tartaglia, Phys. Rev. Lett. **93**, 055701 (2004).
[29] J. Bosse and S. D. Wilke, Phys. Rev. Lett. **80**, 1260 (1998).
[30] S. D. Wilke and J. Bosse, Phys. Rev. E **59**, 1968 (1999).
[31] S. K. Lai and S. Y. Chang, Phys. Rev. B **51**, 12869 (1995).